Eradicating Infecting Bacteria while Maintaining Tissue Integration on Photothermal Nanoparticle-Coated Titanium Surfaces

Ren, Xiaoxiang; Gao, Ruifang; van der Mei, Henny C.; Ren, Yijin; Peterson, Brandon W.; Busscher, Henk J.

Published in:
ACS Applied Materials & Interfaces

DOI:
10.1021/acsami.0c08592

Publication date:
2020

ACS APPLIED MATERIALS & INTERFACES

www.acsami.org

Research Article

Eradicating Infecting Bacteria while Maintaining Tissue Integration on Photothermal Nanoparticle-Coated Titanium Surfaces

Xiaoxiang Ren,[‖] Ruifang Gao,[‖] Henny C. van der Mei,* Yijin Ren, Brandon W. Peterson, and Henk J. Busscher

Cite This: *ACS Appl. Mater. Interfaces* 2020, 12, 34610–34619

Read Online

ACCESS | Metrics & More | Article Recommendations | Supporting Information

ABSTRACT: Photothermal nanoparticles locally release heat when irradiated by near-infrared (NIR). Clinical applications initially involved tumor treatment, but currently extend toward bacterial infection control. Applications toward much smaller, micrometer-sized bacterial infections, however, bear the risk of collateral damage by dissipating heat into tissues surrounding an infection site. This can become a complication when photothermal nanoparticle coatings are clinically applied on biomaterial surfaces requiring tissue integration, such as titanium-made, bone-anchored dental implants. Dental implants can fail due to infection in the pocket formed between the implant screw and the surrounding soft tissue ("peri-implantitis"). We address the hitherto neglected potential complication of collateral tissue damage by evaluating photothermal, polydopamine nanoparticle (PDA-NP) coatings on titanium surfaces in different coculture models. NIR irradiation of PDA-NP-coated (200 $\mu g/cm^2$) titanium surfaces with adhering *Staphylococcus aureus* killed staphylococci within an irradiation time window of around 3 min. Alternatively, when covered with human gingival fibroblasts, this irradiation time window maintained surface coverage by fibroblasts. Contaminating staphylococci on PDA-NP-coated titanium surfaces, as can be per-operatively introduced, reduced surface coverage by fibroblasts, and this could be prevented by NIR irradiation for 5 min or longer prior to allowing fibroblasts to adhere and grow. Negative impacts of early postoperative staphylococcal challenges to an existing fibroblast layer covering a coated surface were maximally prevented by 3 min NIR irradiation. Longer irradiation times caused collateral fibroblast damage. Late postoperative staphylococcal challenges to a protective keratinocyte layer covering a fibroblast layer required 10 min NIR irradiation for adverting a staphylococcal challenge. This is longer than foreseen from monoculture studies because of additional heat uptake by the keratinocyte layer. Summarizing, photothermal treatment of biomaterial-associated infection requires precise timing of NIR irradiation to prevent collateral damage to tissues surrounding the infection site.

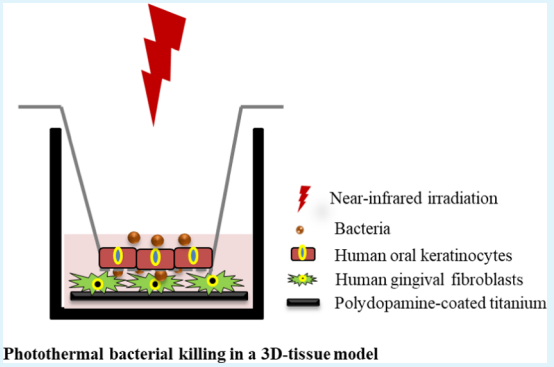

Photothermal bacterial killing in a 3D-tissue model

KEYWORDS: *photothermal therapy, dental implant, coculture model, peri-implantitis, 3D tissue model*

INTRODUCTION

Photothermal therapy (PTT) is highly considered as an alternative bacterial infection control strategy in an era that alludes the end of antibiotic treatment of infection.[1,2] In a pessimistic scenario, infection by antimicrobial-resistant bacteria threatens to become the number one cause of death in the year 2050.[3] Photothermal nanoparticles locally release heat when photoactivated at suitable near-infrared (NIR) wavelengths.[4] The use of PTT in medicine has originated as an antitumor strategy[5−7] and is currently finding its way toward bacterial infection control. As a clear advantage, PTT may be expected to work indiscriminately toward different bacterial strains, regardless of Gram character or antibiotic resistance. Indeed, photothermal copper sulfide nanoclusters effectively killed planktonic levofloxacin-resistant *Staphylococcus aureus*, *Escherichia coli*, *Pseudomonas aeruginosa*, and *Bacillus amyloliquefaciens*,[8] while photothermal *N*-vinylpolycaprolactam-gold nanorods killed planktonic *E. coli*, *Acinetobacter baumannii*, and *Enterococcus faecalis*.[9] However, photothermal killing of planktonic bacteria depends heavily on the ratio of photothermal nanoparticle and bacterial concentration, along with the suspension volume in which heat generated is dissipated.

Clinically, bacterial infections are seldom caused by planktonic bacteria but mainly by bacteria in a biofilm mode of growth, in which bacteria adhere and adapt themselves to the substratum surface by matrix production.[10] "Surface" in this definition can either mean the surface of other bacteria,

Received: May 11, 2020
Accepted: July 7, 2020
Published: July 7, 2020

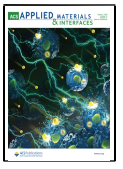

https://dx.doi.org/10.1021/acsami.0c08592
ACS Appl. Mater. Interfaces 2020, 12, 34610–34619

tissue cells, teeth, or implanted biomaterials (joint prostheses, ocular or dental implants, and many others). Effective PTT of bacterial infections requires targeting of photothermal nanoparticles to the infection site and precise NIR irradiation. Modification of photothermal nanoparticles, such as by zwitterionic, pH-responsive molecules, to target photothermal nanoparticles to a bacterial infection site is not trivial, however requiring sophisticated chemistry.[11] Moreover, bacterial infection sites are orders of magnitude smaller in size than tumors,[12] which makes precise NIR irradiation more difficult, while heat dissipation into surrounding tissues may cause collateral tissue damage, which is less critical in control of larger-sized tumors.

The need for targeting photothermal nanoparticles to an infection site can be circumvented when photothermal nanoparticles are applied as a coating on biomaterial implants.[4,13−15] Bacterial challenges form the main cause of failure of biomaterial implants because biomaterial-associated infections are particularly hard to treat with antimicrobials, including antibiotics.[16] The use of NIR irradiation of photothermal nanoparticle coatings to kill infecting bacteria on an implant surface bears the risk of collateral damage to tissue cells integrating the implant. Tissue integration is known to provide the best protection against postoperative infection of biomaterials implants, as arising, e.g., from invasive surgery or trauma.[17] Hitherto, preserving tissue integration of a biomaterials implant has been grossly neglected in the development of photothermal nanoparticles as a novel infection control strategy, possibly by a lack of suitable in vitro models. Suitable models for evaluating photothermal nanoparticles as a novel infection control strategy need not only involve monoculture studies with bacteria or cells but also biculture studies with simultaneous involvement of bacteria and cells, and preferably possess three-dimensional (3D) features to account for the dissipation of heat generated to tissues surrounding an infection site.

Recently, we published a 3D tissue infection model mimicking the soft tissue seal around a dental implant, arguably representing the most frequently applied biomaterial implants.[18] A dental implant consists of a titanium screw and a supragingival part. The implant screw penetrates the gingiva to become anchored in the jaw bone. Composite tooth structures are subsequently attached to the supragingival part of the screw. Dental implants are prone to infection ("peri-implantitis") that occurs in the pocket formed between the implant screw and surrounding soft tissue. Formation of a soft tissue seal consisting of fibroblasts covered with keratinocytes closely adhering to the implant surface protects the osseo-integrated implant screw against bacterial challenges.[19] The peri-implantitis model was setup by growing keratinocytes on a membrane filter in a transwell system, while fibroblasts were adhering to a titanium surface underneath the membrane. Keratinocytes could directly contact the fibroblast underneath the membrane, as an essential feature of 3D tissue models.[20] In the model, bacterial challenges could either be applied as a contamination on the biomaterial surface as in per-operative infections[21] or adhered to the keratinocyte seal above the fibroblasts as in postoperative infections during different stages of healing.[22]

In this paper, we describe the preparation of a NIR-activatable, polydopamine nanoparticle (PDA-NP) coating on titanium with the aim of deriving photothermal conditions for the prevention and treatment of biomaterial-associated infections that maintain tissue integration. To this end, photothermal nanoparticle coatings will be evaluated in various mono- and biculture models, including the above-described 3D tissue infection model of peri-implantitis. Tissue integration will be challenged with *S. aureus* in a per- and postoperative infection modes, evaluating both bacterial killing and collateral damage to fibroblasts integrating the surface. *S. aureus* was chosen as a pathogen, as it is emerging as a causative pathogen in peri-implantitis.[23] Polydopamine (PDA) photothermal nanoparticles (NPs) were selected for coating titanium surfaces because of their good biocompatibility,[24] biodegradability,[25] and strong NIR absorption.[26] Results will point to optimal NIR irradiation times for stimulating and maintaining tissue integration while eradicating infectious bacteria. Although carried out in an oral peri-implantitis model, results bear equal relevance to other biomaterial implants applied in the human body that require tissue integration, such as percutaneous orthopedic screws, bone-anchored joint prostheses, or hearing aids.

EXPERIMENTAL SECTION

Preparation of a Photothermal Polydopamine Nanoparticle Coating on Titanium Surfaces and Its Characterization. Photothermal PDA-NPs were synthesized as described before.[27] Briefly, 7 mL of NH_4OH (28−30%) was mixed with 40 mL of absolute ethanol and 90 mL of demineralized water under mild stirring at 30 °C for 30 min. Then, 10 mL of dopamine (50 mg/mL) solution was added to the solution and stirred for 24 h at 30 °C to allow formation of PDA-NPs. The PDA-NPs were harvested by centrifugation (10 000*g*, 10 min, 20 °C) and washed three times with 96% ethanol, suspended in deionized water, and stored at 4 °C for further use. The morphology of PDA-NPs was examined using a Hitachi G-120 transmission electron microscope operated at 120 kV. To this end, 20 μL of PDA-NP suspension (20 μg/mL) in water was dropped onto a carbon-covered copper grid and dried at 60 °C for 30 min prior to insertion in the microscope. The diameter of the PDA-NPs was measured using a Zetasizer Nano-ZS (Malvern Instruments, Worcestershire, U.K.). Titanium samples (4 × 4 × 1 mm^3) were provided by Salomon's Metalen (Groningen, The Netherlands) and washed with 9 mL of NH_4OH and 9 mL of H_2O_2 in 30 mL of water and heated to 65 °C for 20 min. Next, titanium samples were washed with demineralized water and dried with nitrogen gas. Finally, 4.6 μL of PDA-NP suspension (7 mg/mL) in water was deposited on the titanium surfaces (0.16 cm^2) to obtain different surface concentrations up to 800 $\mu g/cm^2$ PDA-NPs and samples were dried in the oven at 60 °C.

The presence of a PDA-NP coating on titanium samples was demonstrated using scanning electron microscopy (SEM) and X-ray photoelectron spectroscopy (XPS). For SEM, titanium surfaces prior to and after PDA-NP coating were examined using a Zeiss Supra 55 microscope (Carl Zeiss, Germany) at an accelerating voltage of 10 kV. Prior to microscopy, surfaces were spray-coated with a 10 nm thick gold layer.

For XPS, a Surface Science Instrument (Mountain View, CA), equipped with an aluminum anode (10 kV, 22 mA) and a quartz monochromator, was employed. The angle of photoelectron collection was 55° with the sample surface, and the electron flood gun was set at 14 eV. A survey scan over a binding energy range of 1100 eV was made with a 1000 × 250 μm^2 spot and a pass energy of 150 eV. Binding energies were determined by setting the binding energy of the C_{1s} peak (carbon bound to carbon) to 284.8 eV.

Photothermal Effects of PDA-NP-Coated Titanium Surfaces. To determine photothermal effects of PDA-NP-coated titanium surfaces, different volumes of water, phosphate-buffered saline (PBS, 10 mM potassium phosphate, 150 mM NaCl, pH 7.0), and DMEM-HG medium ranging from 10 to 600 μL were added to PDA-NP-coated (200 $\mu g/cm^2$) titanium samples in a 24-well plate. Each sample

https://dx.doi.org/10.1021/acsami.0c08592
ACS Appl. Mater. Interfaces 2020, 12, 34610−34619

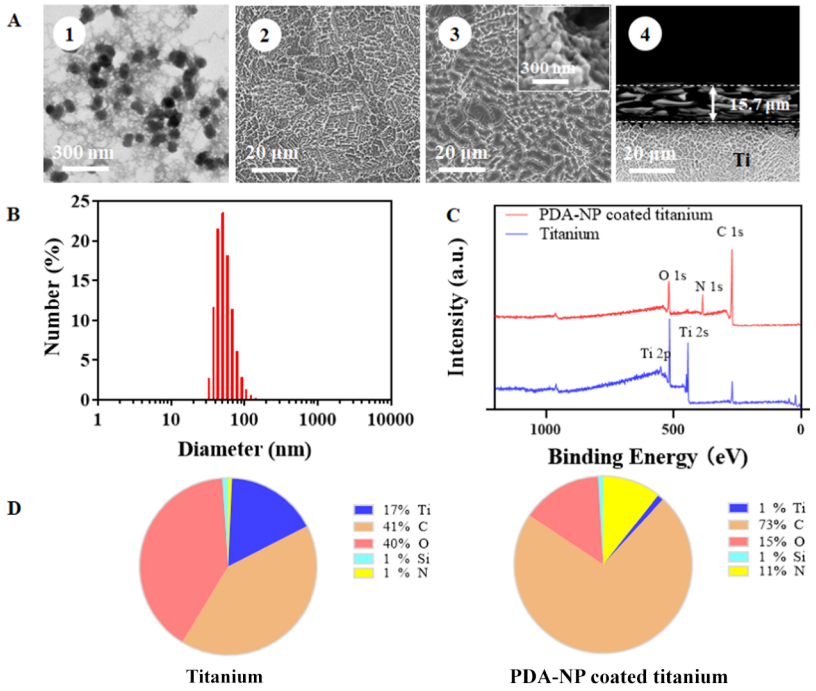

Figure 1. Characterization of titanium and PDA-NP-coated titanium samples. (A) Electron micrographs of PDA-NPs (TEM, panel 1), uncoated, and PDA-NP-coated titanium surfaces (SEM, panels 2 and 3, respectively) and a cross-sectional scanning electron micrograph of the coating (panel 4). The inset in panel 3 shows aggregates of PDA-NPs in the coating. (B) Diameter of PDA-NPs measured using dynamic light scattering (DLS). (C) XPS spectra of uncoated and PDA-NP-coated (200 μg/cm^2) titanium. (D) Elemental surface composition determined using X-ray photoelectron spectroscopy (XPS) of uncoated and PDA-NP-coated titanium samples.

was NIR-irradiated for 10 min at 808 nm (Thorlabs, Newton, NJ) at a power density of 1 W/cm^2. During irradiation, the temperature was recorded using an infrared imaging camera (Fluke TiX580 Infrared Camera, Eindhoven, The Netherlands), imaging the entire sample surface.

Integration of PDA-NP-Coated Titanium Surfaces by Human Gingival Fibroblasts (HGFs) in Monoculture. Human gingival fibroblasts (HGFs) were obtained from the American Type Culture Collection (HGF-1, ATCC-CRL-2014, Manassas) and grown in Dulbecco's modified Eagle's medium (DMEM-HG) supplemented with 10% fetal bovine serum (FBS, Invitrogen, Breda, The Netherlands) at 37 °C in 5% CO_2. Cells from passages 15−25 were used. HGFs (100 μL, 1 × 10^5 HGF/mL) were seeded on sterile PDA-NP-coated titanium samples with different surface concentrations of PDA-NPs in a 96-well plate and incubated at 37 °C in 5% CO_2. After 72 h of growth, the HGF cells were stained with phalloidin-TRITC and DAPI and analyzed using a fluorescence microscope (Leica DM4000, Leica Microsystems Ltd., Wetzlar, Germany). The surface coverage and number of cells per unit area were subsequently derived from the images using image J software.

HGF Integration and Staphylococcal Killing upon NIR Irradiation of PDA-NP-Coated Titanium Surfaces in Respective Monocultures. To observe photothermal effects on HGF integration of PDA-NP-coated titanium surfaces after NIR irradiation, HGFs were grown in monoculture on PDA-NP-coated (200 μg/cm^2) titanium surfaces for 48 h, essentially as described above. After 48 h, the samples were transferred to a 24-well plate and immersed in different volumes of the DMEM-HG medium (between 10 and 600 μL). These volumes encompass the salivary volume embracing a tooth surface (21−100 μL)[28] and are slightly larger than the volume of the embracing crevicular fluid, depending on the periodontal status of a patient (0.12−0.93 μL).[29] Subsequently, samples were irradiated at 808 nm (1 W/cm^2) for 1, 3, 5, and 10 min. After irradiation, cell growth was allowed for 24 h, after which the surface coverage by HGFs was determined, as described above (Integration of PDA-NP-Coated Titanium Surfaces by Human Gingival Fibroblasts (HGFs) in Monoculture Section).

For photothermal bacterial killing, *S. aureus* ATCC12600 was inoculated onto blood agar plates and incubated at 37 °C. After 16 h, one colony was transferred in 10 mL of tryptone soya broth (TSB, OXOID, Basingstoke, UK) and incubated for 24 h at 37 °C. Subsequently, 10 mL of bacterial culture was added to 200 mL of growth medium and incubated for 16 h at 37 °C. Then, staphylococci were harvested by centrifugation at 6300*g* for 5 min at 10 °C, washed twice with sterile PBS, and suspended in PBS. Finally, the staphylococcal suspension was sonicated (3 × 10 s at 30 W) to break bacterial aggregates in an ice/water bath. The bacterial concentration in suspension was enumerated in a Bürker−Türk counting chamber, and the suspension was further diluted in PBS to a concentration of 5 × 10^4 bacteria per mL.

Staphylococci were adhered to a PDA-NP-coated (200 μg/cm^2) titanium surface by adding 1 mL of bacterial suspension into 24-well plates containing a PDA-NP-coated titanium sample. After bacterial sedimentation for 1 h, samples were washed with PBS and transferred into a new well and NIR-irradiated, as described above for HGFs in monoculture. After irradiation, the samples were placed on a hydrated Petrifilm Rapid Aerobic Count (RAC) plate (3M Microbiology, St. Paul, Minnesota) for culturing of viable staphylococci. The Petrifilm plating system was incubated for 48 h at 37 °C, after which the colonies formed were enumerated. Staphylococcal killing was expressed with respect to the number of colony-forming units (CFUs) observed on samples in the absence of NIR irradiation.

Tissue Integration of PDA-NP-Coated Titanium Surfaces upon Staphylococcal Challenges and NIR Irradiation in Bicultures and in a 3D Tissue Infection Model. Staphylococcal challenges were applied to PDA-NP-coated titanium surfaces to mimic different stages of healing. To mimic per-operative contamination prior to tissue integration, 1 mL of staphylococcal suspension (5 × 10^4 mL^{-1}) in PBS was added to a PDA-NP-coated (200 μg/cm^2) titanium surface in a 24-well plate and bacteria were allowed to sediment for 1 h. After 1 h, the samples were transferred to a new well, washed three times with PBS, yielding approximately 1 × 10^3 bacteria/cm^2 on the implant surface, and again transferred to a new well. Different volumes of the DMEM-HG medium (10, 50 and

https://dx.doi.org/10.1021/acsami.0c08592
ACS Appl. Mater. Interfaces 2020, 12, 34610−34619

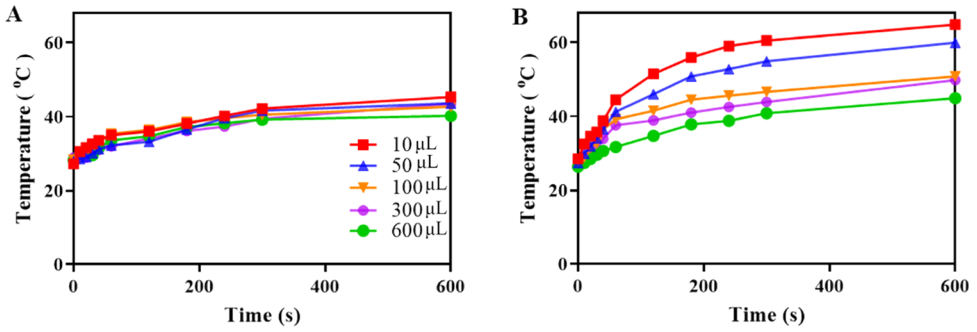

Figure 2. Photothermal effects of PDA-NP coated (200 $\mu g/cm^2$) titanium samples. (A) Temperature of titanium as a function of NIR irradiation time at 808 nm (1 W/cm^2) with different volumes of the DMEM-HG medium above an uncoated titanium sample. (B) Same as (A) but for PDA-NP-coated titanium samples.

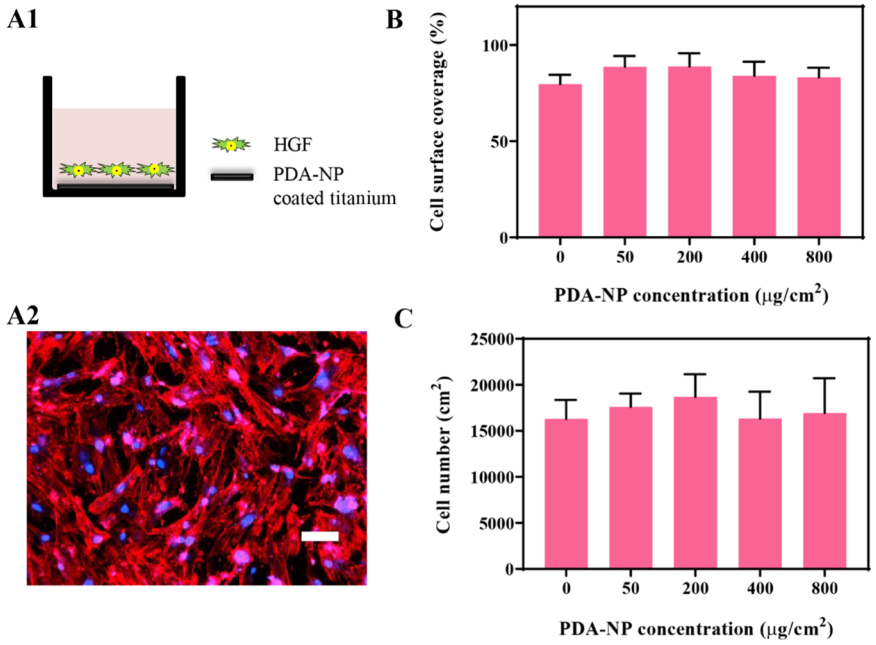

Figure 3. Interaction of HGFs with PDA-NP-coated titanium surfaces in monoculture. (A) Schematics of the monoculture experiments carried out (A1) and a fluorescence image (A2) of DAPI/TRITC-stained HGFs on uncoated titanium, showing red fluorescent skeleton and blue fluorescent nucleus staining. The scale bar represents 100 μm. (B) Surface coverage by adhering HGFs after 72 h of growth on titanium surfaces with different surface concentrations of PDA-NPs (0 $\mu g/cm^2$ indicates the absence of PDA-NPs). (C) Number of adhering HGFs per unit surface area after 72 h of growth on titanium surfaces with different surface concentrations of PDA-NPs. Error bars denote SEM over three experiments with separately cultured cells. There are no statistically significant differences in the cell surface coverage or the cell number at different PDA-NP concentrations ($p > 0.05$).

100 μL) were added on the samples and NIR-irradiated (808 nm) at a power density of 1 W/cm^2 for different times. Subsequently, the samples were transferred to a 96-well plate, 100 μL of HGF suspension of (1×10^5 mL^{-1}) was added, and the well plate was incubated at 37 °C in 5% CO_2. After 24 h of growth, HGFs were stained and analyzed as described before.

In biculture mimicking an early postoperative bacterial contamination before the development of a human oral keratinocyte (HOK) sealing, but with fibroblasts in direct contact with an implant surface, a 48 h grown HGF layer on the samples was challenged by adding 1 mL of *S. aureus* suspension in PBS (5×10^4 mL^{-1}) and allowing sedimentation for 1 h. After 1 h, the samples were transferred to a new well, washed three times with PBS, and transferred again to a new well. Then, different volumes of the DMEM-HG medium (10, 50, and 100 μL) were added on the samples, and the samples were NIR-irradiated at a power density of 1 W/cm^2 for different times. After irradiation, 1 mL of DMEM-HG medium was added and the samples with bacteria and cells were incubated at 37 °C in 5% CO_2. After 24 h of growth, the HGFs were stained and analyzed, as described before.

In a late, postoperative infection model, mimicking a staphylococcal challenge to a fully developed soft tissue seal around an implant, a 3D tissue infection model was used. HOKs were purchased from ScienCell (Carlsbad, CA) and grown in Oral Keratinocyte Medium (OKM, ScienCell) supplemented with Oral Keratinocyte Growth Supplement at 37 °C in 5% CO_2. Cells from passages 3−5 were used in this study. HOKs (100 μL) suspended in OKM (5×10^5 mL^{-1}) were seeded on the transwell membrane (PET transparent, Greiner Bio-One, Frickenhausen, Germany) and incubated for 48 h at 37 °C in 5% CO_2. After 48 h, the cell culture medium was removed, 100 μL of *S. aureus* suspension in PBS (5×10^4 mL^{-1}) was added to the transwell, and staphylococci were allowed to sediment for 1 h. After 1 h, the membranes with adhering HOKs were washed three times with PBS and transferred to a new well containing a PDA-NP-coated titanium sample covered with a layer of HGFs, grown as described above. Different volumes (10, 50, and 100 μL) of the mixed cell culture medium (DMEM-HG and OKM, in a 1:1 ratio[30]) were added to the transwell and the well was NIR-irradiated (808 nm) at a power density of 1 W/cm^2 for different times. After irradiation, 600

https://dx.doi.org/10.1021/acsami.0c08592
ACS Appl. Mater. Interfaces 2020, 12, 34610−34619

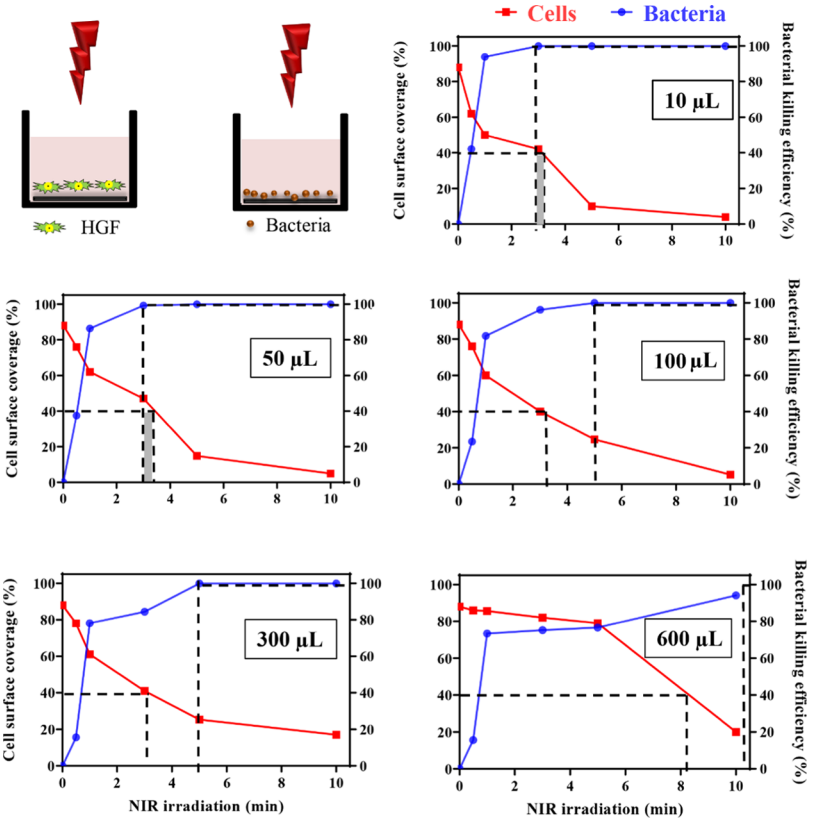

Figure 4. Surface coverage by HGFs and killing of *S. aureus* ATCC12600 upon NIR irradiation (1 W/cm^2, 808 nm) of PDA-NP-coated (200 μg/cm^2) titanium surfaces in monocultures as a function of irradiation time. Samples were immersed in different volumes of the DMEM-HG medium and PBS for HGFs and staphylococci, respectively (see schematics). The dotted lines indicate NIR irradiation times considered acceptable for maintaining tissue integration (>40% cell surface coverage; data in red) and meaningful bacterial killing (>99.9%; data in blue). Gray shading represents the window of acceptable irradiation times, based on both criteria.

μL of mixed cell culture medium was added to the well containing the HGF-covered samples and 100 μL of mixed cell culture medium was added to the transwell containing HOKs and bacteria. After 24 h incubation at 37 °C in 5% CO_2, HGFs were stained and analyzed, as described before.

Statistical Analyses. All data were plotted in Graphpad Prism and Origin. One-way analysis of variance (ANOVA) with a Bonferroni posthoc test was employed using Graphpad Prism version 7.0 software to determine the statistical significance of relevant differences. A value of p <0.05 was considered statistically significant.

RESULTS

Characterization of PDA-NPs and PDA-NP-Coated Titanium Surfaces. PDA-NPs had an average diameter of 52 nm, with a diameter ranging between 38 and 79 nm over 5−95% of the distribution (Figure 1A, panel 1 and Figure 1B). The PDA-NP-coated titanium surface showed clearly a different, more coarse surface structure than the uncoated titanium surface (Figure 1A, compare panels 2 and 3), probably due to aggregation of PDA-NP in the coating (see Figure 1A, inset of panel 3). The PDA-NP coating had a thickness of 15.7 μm (Figure 1A, panel 4). XPS spectra of uncoated and coated titanium surfaces (Figure 1C) demonstrated titanium and oxygen in a ratio of 1:2 (Figure 1D), indicating the presence of an oxide skin on the titanium. XPS furthermore confirmed the presence of PDA on PDA-NP-coated titanium surfaces (Figure 1D), as concluded from the decrease in titanium and oxygen presence, concurrent with an increased presence of nitrogen as compared with uncoated titanium. Nitrogen and oxygen on PDA-NP-coated titanium were present in equal percentages.

Heat Generation by PDA-NP Coatings on Titanium. Previously, we have demonstrated that the light-to-heat conversion efficiency of our PDA-NPs amounted to 21%.[31] NIR irradiation of uncoated titanium samples immersed in different volumes of the DMEM-HG medium yielded a minor light-to-heat conversion (Figure 2A) of up to 16 °C after 10 min in the presence of 10 μL of DMEM-HG medium. Under identical conditions, PDA-NP-coated (200 μg/cm^2) titanium gave an increase of 36 °C (Figure 2B). Dissipation of the heat generated by PDA-NPs on titanium samples when immersed in larger fluid volumes yielded smaller temperature increases. Photothermal effects in water or PBS were similar to those observed in medium (Figure S1).

Integration of PDA-NP-Coated Titanium Surfaces by HGFs in Monoculture. HGFs spread and adhered well on uncoated titanium (Figure 3A) as well as on PDA-NP-coated titanium surfaces. The cell surface coverage (Figure 3B) as a main parameter to quantify tissue integration of an implant surface and the cell number (Figure 3C) were statistically similar for all PDA-NP-coated surfaces, regardless of the PDA-NP surface concentration.

Tissue Integration versus Bacterial Killing upon NIR Irradiation of PDA-NP-Coated Titanium Surfaces in Monocultures. NIR irradiation of PDA-NP-coated titanium surfaces should yield a temperature increase that is high enough to kill infecting bacteria and at the same time maintains tissue integration. Therefore, explorative experiments were first

https://dx.doi.org/10.1021/acsami.0c08592
ACS Appl. Mater. Interfaces 2020, 12, 34610−34619

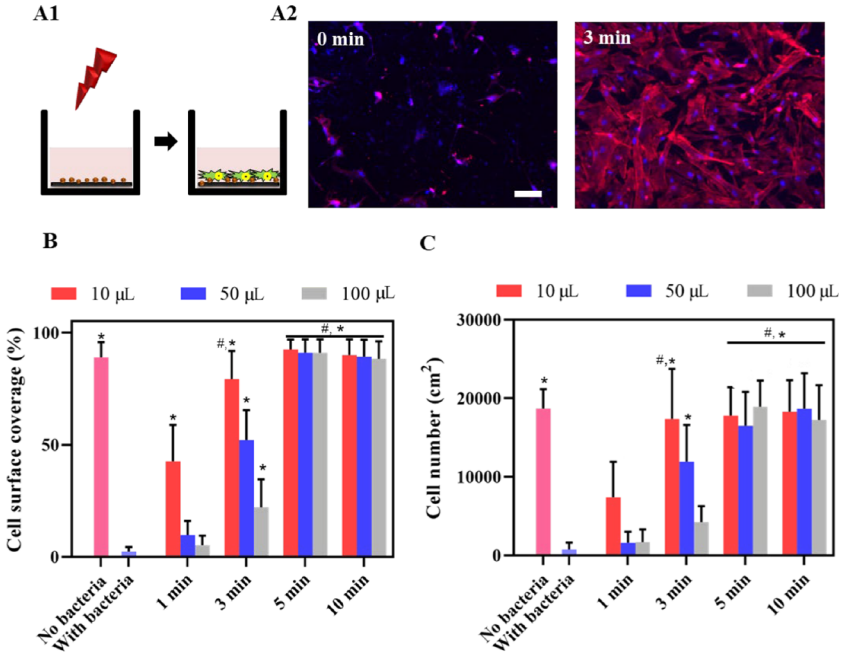

Figure 5. Growth of HGF cells on NIR-irradiated (1 W/cm^2, 808 nm), PDA-NP-coated (200 μg/cm^2) titanium surfaces in a per-operative contamination model. (A) Schematics of bicultures for mimicking per-operative contamination (A1), in which the implant surface is contaminated with *S. aureus* ATCC12600 (1 × 10^3 CFU/cm^2) and irradiated before tissue integration by HGFs. Fluorescence images (A2) represent DAPI/TRITC-stained HGF cells grown for 24 h on *S. aureus*-contaminated, PDA-NP-coated titanium surfaces, in the absence (0 min) and presence of 3 min irradiation (samples immersed in 10 μL of DMEM-HG medium). Red fluorescence indicates skeleton spreading, and blue fluorescence indicates HGF nuclei. The scale bar represents 100 μm. (B) Surface coverage by adhering HGFs on bacteria-contaminated, PDA-NP-coated titanium surfaces in the absence (0 min) and presence of irradiation while immersed in different DMEM-HG volumes. (C) Same as (B) but for the number of adhering HGFs per unit area. Error bars denote SEM over three experiments with separately cultured cells. * Denotes a significant improvement, i.e., a significant decrease upon NIR irradiation ($p < 0.05$), compared with staphylococcal contamination in the absence of NIR irradiation. # Denotes similarity, i.e., no significant difference in the presence of staphylococcal contamination and after NIR irradiation ($p > 0.05$), compared with the absence of staphylococcal contamination.

done at different NIR irradiation times at an intermediate PDA-NP surface concentration (200 μg/cm^2), immersing the titanium samples in different fluid volumes. In this exploratory phase, bacterial killing and tissue integration were separately assessed in monocultures. The surface coverage by HGFs decreased as a function of increasing NIR irradiation time, particularly when samples were immersed in small fluid volumes (Figure 4). Oppositely, staphylococcal killing increased as a function of increasing NIR irradiation time, particularly when immersed in smaller fluid volumes (see also Figure 4 and Table S1 for numerical details). Subsequently, these graphs were employed to derive NIR irradiation times that yielded acceptable tissue coverage and bacterial killing. A surface coverage by tissue cells of minimally 40% has been demonstrated in the past to allow tissue cells to win the race for the surface from contaminating bacteria.[22] Hence, acceptable NIR irradiation times should leave at least 40% surface coverage by tissue cells. Analogously, antimicrobials with potential clinical efficacy should minimally demonstrate 99.9% (or 3 log-units) bacterial killing.[32] This yielded a second criterion for acceptable NIR irradiation times. Based on these criteria, this exploratory study showed a narrow window of possible NIR irradiation times of around 3 min (Figure 4) for samples immersed in 10 or 50 μL, which were used for further experiments to more precisely determine the window of possible NIR irradiation times in coculture studies. Based on Figure 2, these conditions would yield a temperature increase to 56 or 51 °C for an immersion volume of 10 or 50 μL, respectively.

Tissue Integration of NIR-Irradiated, PDA-NP-Coated Titanium Surfaces upon Staphylococcal Challenges in Bicultures and in a 3D Tissue Infection Model. The effect of NIR irradiation was measured in pre- and postoperative infection models, mimicking different stages of healing. In a per-operative contamination model (Figure 5A), the presence of staphylococci adhering in low numbers (1 × 10^3 CFU/cm^2) caused a significant decrease in the surface coverage (Figure 5B) and the number of adhering HGFs (Figure 5C). Photothermal killing of adhering staphylococci prior to tissue integration yielded significant improvement of tissue integration to the level observed in the absence of staphylococcal contamination (Figures 5B,C) when irradiated with NIR for a minimum of 5 min, regardless of the fluid volume.

In an early postoperative contamination model, in which an HGF layer is formed but not yet sealed with a layer of protecting keratinocytes, tissue integration was also entirely lost upon a *S. aureus* challenge (Figure 6A). NIR irradiation improved tissue integration upon a staphylococcal challenge when applied for 3 min (Figure 6B,C), except for the largest immersion fluid volume (100 μL). A shorter irradiation time was insufficient because it allowed survival of staphylococci, while a longer irradiation times caused collateral damage to the HGFs integrating the surface.

In a late 3D tissue postoperative infection model, in which HGFs are protected by a keratinocyte seal, a staphylococcal challenge was far less harmful to tissue integration of the titanium surface than in the absence of the protective keratinocyte seal (compare Figures 6 and 7). NIR irradiation

https://dx.doi.org/10.1021/acsami.0c08592
ACS Appl. Mater. Interfaces 2020, 12, 34610−34619

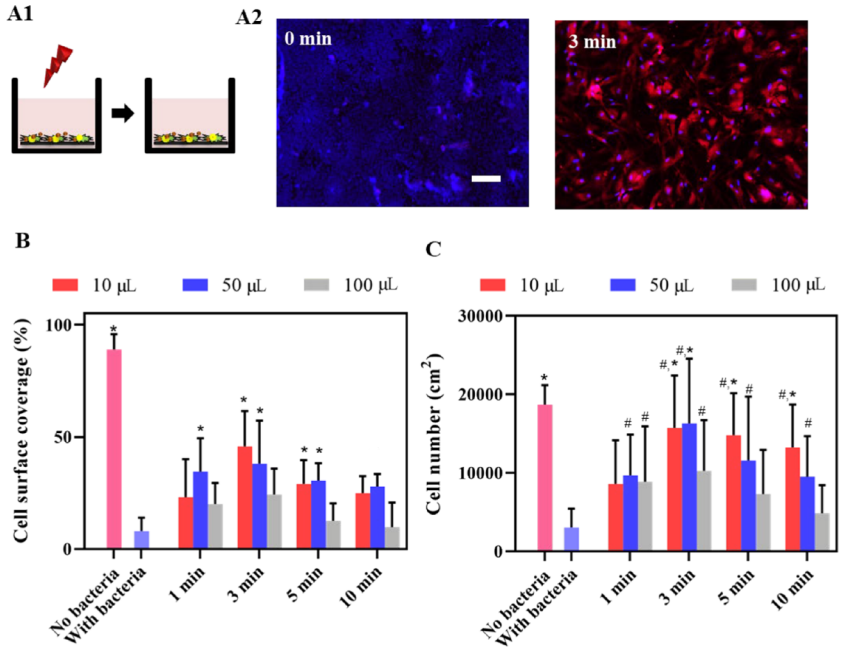

Figure 6. Growth of HGF cells on NIR-irradiated (1 W/cm^2, 808 nm), PDA-NP-coated (200 μg/cm^2) titanium surfaces after a challenge by *S. aureus* ATCC12600 in an early postoperative contamination model in the absence of a keratinocyte seal. (A) Schematics of the early postoperative contamination model (A1), in which an HGF layer on an implant surface in the absence of a protective keratinocyte seal is challenged with *S. aureus* ATCC12600 (1×10^3 CFU/cm^2) and irradiated, followed by 24 h of further growth of the HGF layer. Fluorescence images (A2) of DAPI/TRITC-stained HGF cells further grown after an *S. aureus* challenge, in the absence (0 min) and presence of 3 min irradiation (samples immersed in 10 μL of DMEM-HG medium). Red fluorescence indicates skeleton spreading, and blue fluorescence indicates HGF nuclei. The scale bar represents 100 μm. (B) Surface coverage by adhering HGFs on PDA-NP-coated titanium surfaces after a staphylococcal challenge in the absence (0 min) and presence of irradiation while immersed in different DMEM-HG volumes. (C) Same as (B) but for the number of adhering HGFs per unit area. Error bars denote SEM over three experiments with separately cultured cells. * Denotes a significant improvement, i.e., a significant difference upon NIR irradiation ($p < 0.05$), compared with staphylococcal contamination in the absence of NIR irradiation. # Denotes similarity, i.e., no significant difference in the presence of staphylococcal contamination and after NIR irradiation ($p > 0.05$), compared with the absence of staphylococcal contamination.

for 10 min maintained the surface coverage (Figure 7B) and restored the cell number (Figure 7C) to the level observed in the absence of a staphylococcal challenge except for the largest immersion fluid volume (100 μL). NIR irradiation was advantageous only upon relatively long irradiation times (10 min) due to heat dissipation in the additional volume of the keratinocyte seal.

DISCUSSION

In this article, we show that both the volume of immersing body fluids and the volume of tissue surrounding an infectious biofilm can absorb heat to diminish photothermal killing of bacteria by NIR-irradiated nanoparticles. Moreover, this article is the first to show collateral thermal damage to tissues covering an implant surface coated with photothermal nanoparticles. Importantly, this article bases its conclusions on the surface coverage of an implant material as the "crown" parameter in the race for the surface between tissue integration and bacterial colonization.[33] Cell surface coverage is determined by cell spreading and the number of cells per unit area. Cells mostly round up under a bacterial challenge and only detach when they "realize" that the race cannot be won. Thus, when the spreading of an individual cell is less due to bacterial presence, but the total number of cells on a surface stays the same, the cell surface coverage will decrease (see several of the scenarios depicted in Figures 6 and 7).

In the different in vitro models employed here, it is demonstrated that the merits of photothermal bacterial killing without collateral damage to surrounding tissues leave only a narrow NIR irradiation time window. Furthermore, merits heavily depend on whether photothermal treatment is applied as a prophylactic measure in the per-operative phase or as a therapeutic measure in the postoperative phase. In an early per-operative scenario, photothermal treatment only aims to kill bacteria that may have contaminated the implant surface during surgery and collateral tissue damage due to dissipating heat is not important. Bacterial challenges can also arise however, once healing, bone anchoring and the formation of a soft tissue seal, around dental implants, has commenced (early postoperative scenario). Particularly in a bacteria-laden environment as the oral cavity, bacterial challenges during healing are impossible to avoid. Also, once healing is completed and a protective soft tissue seal has been formed with a keratinocyte layer covering fibroblasts (late post-operative scenario), bacterial challenges can be detrimental to an implant. In the latter two cases, we here show that NIR irradiation of implant surfaces coated with photothermal nanoparticles can have beneficial effects on tissue coverage, provided NIR irradiation times are carefully chosen and do not cause collateral photothermal damage to the tissue cells in the soft tissue seal.

Temperatures above 50 °C generally lead to killing of infectious bacteria due to damage to vital proteins and enzymes.[34] Unfortunately, heat-induced denaturation of tissue cell proteins readily occurs already above 40 °C, causing cell injury or death.[35] Relevant to several types of biomaterials

https://dx.doi.org/10.1021/acsami.0c08592
ACS Appl. Mater. Interfaces 2020, 12, 34610−34619

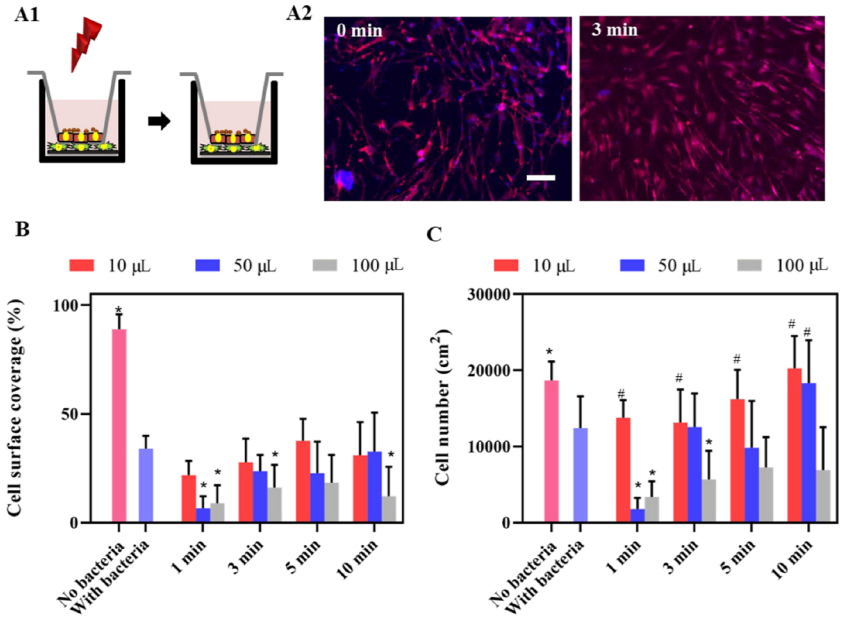

Figure 7. Growth of HGF cells on NIR-irradiated (1 W/cm^2, 808 nm), PDA-NP-coated (200 μg/cm^2) titanium surfaces after a challenge by *S. aureus* ATCC12600 in a late postoperative infection model in which a protective keratinocyte seal is present. (A) Schematics of the late postoperative infection model (A1), in which an HGF layer on an implant surface in the presence of a protective keratinocyte seal is challenged with *S. aureus* ATCC12600 (1 ×10^3 CFU/cm^2) and irradiated, followed by 24 h of further growth of the HGF layer. Fluorescence images (A2) of DAPI/TRITC-stained HGF cells further grown after an *S. aureus* challenge, in the absence (0 min) and in presence of irradiation (samples immersed in 10 μL of DMEM-HG medium). Red fluorescence indicates skeleton spreading, and blue fluorescence indicates HGF nuclei. The scale bar represents 100 μm. (B) Surface coverage by adhering HGF on PDA-NP-coated titanium surfaces after a staphylococcal challenge in the absence (0 min) and presence of NIR irradiation while immersed in different DMEM-HG volumes. (C) Same as (B) but for the number of adhering HGFs per unit area. Error bars denote SEM over three experiments with separately cultured cells. * Denotes a significant difference upon NIR irradiation ($p < 0.05$), compared with staphylococcal contamination in the absence of NIR irradiation. # Denotes similarity, i.e., no significant difference in the presence of staphylococcal contamination and after NIR irradiation ($p > 0.05$), compared with the absence of staphylococcal contamination.

implants, such as dental implants and orthopedic implants requiring anchoring in bones, cortical bone necrosis occurs above 47 °C.[36] Gold-nanorod-coated titanium surfaces reached temperatures of 49 °C upon NIR irradiation for 20 min in a large immersion volume of 1 mL, which maintained viability of osteoblast precursor cells in monoculture but killed only 60% of adhering bacteria, also in monoculture.[4] Gold-nanostar-coated glass induced killing of *S. aureus* biofilms upon NIR irradiation when immersed in 0.5 mL of fluid.[14]

PTT was initially applied for tumor treatment.[37] In clinical tumor treatment, heat dissipation into tissues surrounding a tumor is not an issue because of the relatively large volume of the tumor compared with infection sites.[38] Clinically, for instance, the volume of prostate tumors could be reduced from 49 to 42 cm^3 using gold−silica nanogels.[39] *In vitro* success, however, depends heavily on the immersion fluid volume in which the generated heat dissipates and tumor cells are photothermally treated. In some studies, immersion fluid volumes are clearly mentioned. A study on colorectal cancer cells treated with copper(II) sulfide nanocrystals[40] explicitly reported NIR irradiation time (5 min), power density (33 W/cm^2), and immersion fluid volume (375 μL). However, to our knowledge, many if not most other studies on PTT on tumor cells do not affirmatively report immersion fluid volumes.[41,42] The limitations of not properly reporting immersion fluid volumes exist also in many papers dealing with PTT for bacterial infection control, such as in the evaluation of the photothermal killing of *P. aeruginosa*.[43] Evaluation of a photothermal PDA coating with adhering *S. aureus*, *E. coli*, and *C. albicans*, after removal of the sample from its immersion fluid and after drying before NIR irradiation, yielded only 96, 84, and 93% killing for the respective strains.[44] This is far less than the 3 log-unit reduction in CFUs required for potential clinical efficacy.[32] Air drying is entirely alien to the clinical situation, in which coated implants are in direct contact with body fluids or surrounding tissues that absorb heat. The omission of not properly reporting immersion fluid volumes or accounting for the presence of surrounding tissues into which heat generated during PTT can dissipates leaves many bridges to cross before PTT can be clinically applied in infection control. Use of mono- and biculture models, including 3D tissue infection models, may facilitate easier crossing of these bridges because its use will not only provide measures of bacterial killing but also of collateral heat damage to tissues surrounding an infection site.

CONCLUSIONS

Photothermal killing of infectious bacteria is generally presented in the literature as a success story without side effects. In vitro success can easily be ensured by properly adjusting immersion fluid volumes, but many articles do not clearly report or justify immersion fluid volumes. In this article, we present a photothermal PDA-NP coating for biomaterial implants and show that killing of bacteria contaminating the surface or challenging the protective tissues surrounding an implant critically depends on the immersion volume in which experiments are done. Moreover, we show that photothermal treatment of a biomaterial-associated infection requires precise timing of NIR irradiation to maintain tissue integration, which eventually provides the best long-term protection of a

https://dx.doi.org/10.1021/acsami.0c08592
ACS Appl. Mater. Interfaces 2020, 12, 34610−34619

biomaterial implant against infection. Exact timing depends on whether photothermal treatment is done as a prophylactic measure in the per-operative phase or therapeutically in the postoperative phase. This paper clearly demonstrates the importance of the influence of these important side conditions that need to be taken into account for the clinical translation of photothermal treatment of bacterial infections and biomaterial-associated ones in particular.

■ ASSOCIATED CONTENT

Supporting Information

The Supporting Information is available free of charge at https://pubs.acs.org/doi/10.1021/acsami.0c08592.

Photothermal effects of titanium samples immersed in different fluids and killing of *S. aureus* adhering on PDA-NP-coated titanium surfaces after NIR irradiation (PDF)

■ AUTHOR INFORMATION

Corresponding Author

Henny C. van der Mei − *University of Groningen and University Medical Center Groningen, Department of Biomedical Engineering, 9713 AV Groningen, The Netherlands;* orcid.org/0000-0003-0760-8900; Phone: +31 50 361 6094; Email: h.c.van.der.mei@umcg.nl

Authors

Xiaoxiang Ren − *University of Groningen and University Medical Center Groningen, Department of Biomedical Engineering, 9713 AV Groningen, The Netherlands*

Ruifang Gao − *University of Groningen and University Medical Center Groningen, Department of Biomedical Engineering, 9713 AV Groningen, The Netherlands; College of Chemistry, Chemical Engineering and Materials Science, Soochow University, Suzhou 215123, China*

Yijin Ren − *University of Groningen and University Medical Center Groningen, Department of Orthodontics, 9700 RB Groningen, The Netherlands*

Brandon W. Peterson − *University of Groningen and University Medical Center Groningen, Department of Biomedical Engineering, 9713 AV Groningen, The Netherlands;* orcid.org/0000-0002-8969-3696

Henk J. Busscher − *University of Groningen and University Medical Center Groningen, Department of Biomedical Engineering, 9713 AV Groningen, The Netherlands*

Complete contact information is available at: https://pubs.acs.org/10.1021/acsami.0c08592

Author Contributions

‖X.R. and R.G. contributed equally to this work.

Notes

The authors declare the following competing financial interest(s): H.J.B. is also director-owner of a consulting company SASA BV. The authors declare no potential conflicts of interest with respect to authorship and/or publication of this article. Opinions and assertions contained herein are those of the authors and are not construed as necessarily representing views of the funding organizations or their employer(s).

■ ACKNOWLEDGMENTS

X.R. thanks the China Scholarship Council and W.J. Kolff Institute, UMCG, Groningen, The Netherlands for financial support. The authors were employed by their own organizations.

■ REFERENCES

(1) Jones, K. E.; Patel, N. G.; Levy, M. A.; Storeygard, A.; Balk, D.; Gittleman, J. L.; Daszak, P. Global Trends in Emerging Infectious Diseases. *Nature* **2008**, *451*, 990−993.

(2) Gao, G.; Jiang, Y. W.; Jia, H. R.; Wu, F. G. Near-Infrared Light-Controllable on-Demand Antibiotics Release Using Thermo-Sensitive Hydrogel-Based Drug Reservoir for Combating Bacterial Infection. *Biomaterials* **2019**, *188*, 83−95.

(3) O'Neill, J. *Tackling Drug-Resistant Infections Globally: Final Report and Recommendations*; Review on Antimicrobial Resistance: U.K., 2016.

(4) Yang, T.; Wang, D.; Liu, X. Assembled Gold Nanorods for the Photothermal Killing of Bacteria. *Colloids Surf., B* **2019**, *173*, 833−841.

(5) Lal, S.; Clare, S. E.; Halas, N. J. Nanoshell-Enabled Photothermal Cancer Therapy: Impending Clinical Impact. *Acc. Chem. Res.* **2008**, *41*, 1842−1851.

(6) Abbas, M.; Zou, Q.; Li, S.; Yan, X. Self-Assembled Peptide- and Protein-Based Nanomaterials for Antitumor Photodynamic and Photothermal Therapy. *Adv. Mater.* **2017**, *29*, No. 1605021.

(7) Chen, X.; Yi, Z.; Chen, G.; Ma, X.; Su, W.; Cui, X.; Li, X. DOX-Assisted Functionalization of Green Tea Polyphenol Nanoparticles for Effective Chemo-Photothermal Cancer Therapy. *J. Mater. Chem. B* **2019**, *7*, 4066−4078.

(8) Dai, X.; Zhao, Y.; Yu, Y.; Chen, X.; Wei, X.; Zhang, X.; Li, C. Single Continuous Near-Infrared Laser-Triggered Photodynamic and Photothermal Ablation of Antibiotic-Resistant Bacteria Using Effective Targeted Copper Sulfide Nanoclusters. *ACS Appl. Mater. Interfaces* **2017**, *9*, 30470−30479.

(9) Abdou Mohamed, M. A.; Raeesi, V.; Turner, P. V.; Rebbapragada, A.; Banks, K.; Chan, W. C. W. A Versatile Plasmonic Thermogel for Disinfection of Antimicrobial Resistant Bacteria. *Biomaterials* **2016**, *97*, 154−163.

(10) Hall-Stoodley, L.; Costerton, J. W.; Stoodley, P. Bacterial Biofilms: From the Natural Environment to Infectious Diseases. *Nat. Rev. Microbiol.* **2004**, *2*, 95−108.

(11) Hu, D.; Li, H.; Wang, B.; Ye, Z.; Lei, W.; Jia, F.; Jin, Q.; Ren, K. F.; Ji, J. Surface-Adaptive Gold Nanoparticles with Effective Adherence and Enhanced Photothermal Ablation of Methicillin-Resistant *Staphylococcus aureus* Biofilm. *ACS Nano* **2017**, *11*, 9330−9339.

(12) Cummins, J.; Tangney, M. Bacteria and Tumours: Causative Agents or Opportunistic Inhabitants? *Infect. Agent. Cancer* **2013**, *8*, No. 11.

(13) Alenezi, A.; Hulander, M.; Atefyekta, S.; Andersson, M. Development of a Photon Induced Drug-Delivery Implant Coating. *Mater. Sci. Eng. C* **2019**, *98*, 619−627.

(14) Pallavicini, P.; Donà, A.; Taglietti, A.; Minzioni, P.; Patrini, M.; Dacarro, G.; Chirico, G.; Sironi, L.; Bloise, N.; Visai, L.; Scarabelli, L. Self-Assembled Monolayers of Gold Nanostars: A Convenient Tool for Near-IR Photothermal Biofilm Eradication. *Chem. Commun.* **2014**, *50*, 1969−1971.

(15) Xu, X.; Liu, X.; Tan, L.; Cui, Z.; Yang, X.; Zhu, S.; Li, Z.; Yuan, X.; Zheng, Y.; Yeung, K. W. K.; Chu, P. K.; Wu, S. Controlled-Temperature Photothermal and Oxidative Bacteria Killing and Acceleration of Wound Healing by Polydopamine-Assisted Au-Hydroxyapatite Nanorods. *Acta Biomater.* **2018**, *77*, 352−364.

(16) Busscher, H. J.; Van der Mei, H. C.; Subbiahdoss, G.; Jutte, P. C.; Van den Dungen, J. J. A. M.; Zaat, S. A. J.; Schultz, M. J.; Grainger, D. W. Biomaterial-Associated Infection: Locating the Finish Line in the Race for the Surface. *Sci. Transl. Med.* **2012**, *9*, No. 153rv10.

(17) Werner, S.; Huck, O.; Frisch, B.; Vautier, D.; Elkaim, R.; Voegel, J. C.; Brunel, G.; Tenenbaum, H. The Effect of Micro-structured Surfaces and Laminin-Derived Peptide Coatings on Soft Tissue Interactions with Titanium Dental Implants. *Biomaterials* **2009**, *30*, 2291−2301.

(18) Ren, X.; Van der Mei, H. C.; Ren, Y.; Busscher, H. J. Keratinocytes Protect Soft-Tissue Integration of Dental Implant Materials against Bacterial Challenges in a 3D-Tissue Infection Model. *Acta Biomater.* **2019**, *96*, 237−246.
(19) Zhao, B.; Van der Mei, H. C.; Subbiahdoss, G.; De Vries, J.; Rustema-Abbing, M.; Kuijer, R.; Busscher, H. J.; Ren, Y. Soft Tissue Integration versus Early Biofilm Formation on Different Dental Implant Materials. *Dent. Mater.* **2014**, *30*, 716−727.
(20) Basso, F. G.; Pansani, T. N.; Marcelo, C. L.; de Souza Costa, C. A.; Hebling, J.; Feinberg, S. E. Phenotypic Markers of Oral Keratinocytes Seeded on Two Distinct 3D Oral Mucosa Models. *Toxicol. In Vitro* **2018**, *51*, 34−39.
(21) Subbiahdoss, G.; Kuijer, R.; Grijpma, D. W.; Van der Mei, H. C.; Busscher, H. J. Microbial Biofilm Growth vs. Tissue Integration: "The Race for the Surface" Experimentally Studied. *Acta Biomater.* **2009**, *5*, 1399−1404.
(22) Subbiahdoss, G.; Kuijer, R.; Busscher, H. J.; Van der Mei, H. C. Mammalian Cell Growth versus Biofilm Formation on Biomaterial Surfaces in an *In Vitro* Post-Operative Contamination Model. *Microbiology* **2010**, *156*, 3073−3078.
(23) Albertini, M.; López-Cerero, L.; O'Sullivan, M. G.; Chereguini, C. F.; Ballesta, S.; Ríos, V.; Herrero-Climent, M.; Bullón, P. Assessment of Periodontal and Opportunistic Flora in Patients with Peri-Implantitis. *Clin. Oral Implants Res.* **2015**, *26*, 937−941.
(24) Li, Y.; Jiang, C.; Zhang, D.; Wang, Y.; Ren, X.; Ai, K.; Chen, X.; Lu, L. Targeted Polydopamine Nanoparticles Enable Photoacoustic Imaging Guided Chemo-Photothermal Synergistic Therapy of Tumor. *Acta Biomater.* **2017**, *47*, 124−134.
(25) Bao, X.; Zhao, J.; Sun, J.; Hu, M.; Yang, X. Polydopamine Nanoparticles as Efficient Scavengers for Reactive Oxygen Species in Periodontal Disease. *ACS Nano* **2018**, *12*, 8882−8892.
(26) Zhu, Z.; Su, M. Polydopamine Nanoparticles for Combined Chemo- and Photothermal Cancer Therapy. *Nanomaterials* **2017**, *7*, 160.
(27) Liu, Y.; Ai, K.; Liu, J.; Deng, M.; He, Y.; Lu, L. Dopamine-Melanin Colloidal Nanospheres: An Efficient near-Infrared Photothermal Therapeutic Agent for *In Vivo* Cancer Therapy. *Adv. Mater.* **2013**, *25*, 1353−1359.
(28) Edgar, M.; Dawes, C.; O'Mullane, D. (Eds.), *Saliva and Oral Health*, 3rd ed., British Dental Association: London, 2004.
(29) Attar, N. B.; Banodkar, A. B.; Gaikwad, R. P.; Sethna, G. D.; Patil, C. L.; Simon, S. Evaluation of Gingival Crevicular Fluid Volume in Relation to Clinical Periodontal Status with Periotron 8000. *Int. J. Appl. Dent. Sci.* **2018**, *4*, 68−71.
(30) Sawicki, G.; Marcoux, Y.; Sarkhosh, K.; Tredget, E. E.; Ghahary, A. Interaction of Keratinocytes and Fibroblasts Modulates the Expression of Matrix Metalloproteinases-2 and -9 and Their Inhibitors. *Mol. Cell. Biochem.* **2005**, *269*, 209−216.
(31) Gao, R.; Van der Mei, H. C.; Ren, Y.; Chen, H.; Chen, G.; Busscher, H. J.; Peterson, B. W. Thermo-Resistance of ESKAPE-Panel Pathogens and Eradication and Growth Prevention of an Infectious Biofilm by Photothermal, Polydopamine-Nanoparticles *In Vitro*. 2020. (submitted).
(32) Garcia, L. Tests to Assess Bacterial Activity, In *Clinical Microbiology Procedures Handbook*, 3rd ed.; ASM Press: Washington, pp 89−123.
(33) Gristina, A. G. Biomaterial-centered Infection: Microbial Adhesion Versus Tissue Integration. *Science* **1987**, *237*, 1588−1595.
(34) Wu, M. C.; Deokar, A. R.; Liao, J. H.; Shih, P. Y.; Ling, Y. C. Graphene-Based Photothermal Agent for Rapid and Effective Killing of Bacteria. *ACS Nano* **2013**, *7*, 1281−1290.
(35) Lepock, J. R. Cellular Effects of Hyperthermia: Relevance to the Minimum Dose for Thermal Damage. *Int. J. Hyperth.* **2003**, *19*, 252−266.
(36) Augustin, G.; Davila, S.; Mihoci, K.; Udiljak, T.; Vedrina, D. S.; Antabak, A. Thermal Osteonecrosis and Bone Drilling Parameters Revisited. *Arch. Orthop. Trauma Surg.* **2007**, *128*, 71−77.
(37) Huang, X.; Jain, P. K.; El-Sayed, I. H.; El-Sayed, M. A. Plasmonic Photothermal Therapy (PPTT) Using Gold Nanoparticles. *Lasers Med. Sci.* **2008**, *23*, No. 217.
(38) Bjarnsholt, T.; Alhede, M.; Alhede, M.; Eickhardt-Sørensen, S. R.; Moser, C.; Kühl, M.; Østrup Jensen, P.; Høiby, N. The *In Vivo* Biofilm. *Trends Microbiol.* **2013**, *21*, 466−474.
(39) Rastinehad, A. R.; Anastos, H.; Wajswol, E.; Winoker, J. S.; Sfakianos, J. P.; Doppalapudi, S. K.; Carrick, M. R.; Knauer, C. J.; Taouli, B.; Lewis, S. C.; Tewari, A. K.; Schwartz, J. A.; Canfield, S. E.; George, A. K.; West, J. L.; Halas, N. J. Gold Nanoshell-Localized Photothermal Ablation of Prostate Tumors in a Clinical Pilot Device Study. *Proc. Natl. Acad. Sci. U.S.A.* **2019**, *116*, 18590−18596.
(40) Hessel, C. M.; P. Pattani, V.; Rasch, M.; Panthani, M. G.; Koo, B.; Tunnell, J. W.; Korgel, B. A. Copper Selenide Nanocrystals for Photothermal Therapy. *Nano Lett.* **2011**, *11*, 2560−2566.
(41) El-Sayed, I. H.; Huang, X.; El-Sayed, M. A. Selective Laser Photo-Thermal Therapy of Epithelial Carcinoma Using Anti-EGFR Antibody Conjugated Gold Nanoparticles. *Cancer Lett.* **2006**, *239*, 129−135.
(42) MacKey, M. A.; Ali, M. R. K.; Austin, L. A.; Near, R. D.; El-Sayed, M. A. The Most Effective Gold Nanorod Size for Plasmonic Photothermal Therapy: Theory and *In Vitro* Experiments. *J. Phys. Chem. B* **2014**, *118*, 1319−1326.
(43) Zhao, Y.; Yu, C.; Yu, Y.; Wei, X.; Duan, X.; Dai, X.; Zhang, X. Bioinspired Heteromultivalent Ligand-Decorated Nanotherapeutic for Enhanced Photothermal and Photodynamic Therapy of Antibiotic-Resistant Bacterial Pneumonia. *ACS Appl. Mater. Interfaces* **2019**, *11*, 39648−39661.
(44) Lei, W.; Ren, K.; Chen, T.; Chen, X.; Li, B.; Chang, H.; Ji, J. Polydopamine Nanocoating for Effective Photothermal Killing of Bacteria and Fungus upon Near-Infrared Irradiation. *Adv. Mater. Interfaces* **2016**, *3*, 767.

https://dx.doi.org/10.1021/acsami.0c08592
ACS Appl. Mater. Interfaces 2020, 12, 34610−34619